Effect of roughness on surface plasmon scattering in gold films

1998 J. Phys.: Condens. Matter 10 5503

(http://iopscience.iop.org/0953-8984/10/24/025)

J. Phys.: Condens. Matter **10** (1998) 5503–5513. Printed in the UK PII: S0953-8984(98)91317-0

Effect of roughness on surface plasmon scattering in gold films

A Hoffmann, Z Lenkefi and Z Szentirmay†

Research Institute for Solid State Physics, H-1525 Budapest, PO Box 49, Hungary

Received 3 February 1998, in final form 6 April 1998

Abstract. Attenuated total reflection and rear-side light emission were measured on 50 nm thick gold films evaporated on glass substrates previously coated with LiF layers of 0–500 nm thickness. The complex dielectric constant of metal films was determined as a function of the fluoride thickness. Roughness parameters (σ, δ) were calculated from the angular distribution of the emission intensity and also from atomic force microscope images. Roughness amplitudes (δ) were found to be proportional to the fluoride thickness up to 350 nm, but over this value began to decrease. Both the average grain diameter and the correlation length (σ) increased with the layer thickness in the whole observed range, indicating the flattening out of LiF at large thicknesses. Dielectric functions and surface plasmon wave-vectors of gold layers change drastically under the influence of increasing roughness amplitudes, which effect cannot be quantitatively described by the unmodified Fresnel equations.

1. Introduction

The quality of a thin metal layer is characterized by its optical parameters, e.g. the complex dielectric function which can be determined by normal reflectometry, ellipsometry and if the metal allows surface plasmons by attenuated total reflection (ATR) spectrometry [1]. However, since the natural surface roughness of the substrate and of the layer may drastically influence the measured optical parameters, information on surface roughness is of primary importance for the preparation of any kind of thin film device. In order to study the effect of surface roughness on the optical properties of gold films, we performed ATR measurements on samples whose LiF sublayers were of different thickness, obeying different roughness structures. The principal aim was to study the usefulness of the optical (ATR) and other methods such as atomic force microscopy (AFM) in evaluating roughness parameters.

2. Experiment

Samples were evaporated at 6×10^{-4} Pa pressure on $18 \times 18 \times 1$ mm^3 BK-7 glass substrates, which were pitch polished with standard 60/40 scratch/dig ratio. The evaporation rate was 0.5 nm s^{-1} and 2 nm s^{-1} for gold and LiF, respectively. The thickness of LiF varied from 0 to 500 nm. Substrates were first coated with a given thickness of LiF and then 50 nm of gold was deposited on them in a single step, which resulted in gold layers of exactly the same mass-thickness and structure on every sample.

† Phone: (36)-1-395-9220. Fax: (36)-1-395-9278. E-mail address: szenti@power.szfki.kfki.hu

0953-8984/98/245503+11$19.50

The specular reflectivity of gold films was measured in the x–y plane with a high precision, twin-goniometer ATR reflectometer (described in [2]). Samples were attached to a 100 mm diameter BK-7 semi-cylindrical prism by their glass side with a drop of glycerine immersion liquid (figure 1). Laser light of $\lambda = 632.8$ or 1064 nm wavelength, travelling through the prism, was reflected from the internal surface of the gold film. If the beam was p-polarized (i.e. its electric vector was lying in the plane of reflection), at some angle of incidence θ_0 surface plasmons of the gold/air interface propagating in the x direction were resonantly excited by the evanescent field of the beam. At this angle a dip appeared in the reflectivity curve. A subsequent three-parameter fit of the R–θ curve by the unmodified Fresnel equations resulted in the complex dielectric function $\tilde{\varepsilon} = \varepsilon_r + \mathrm{i}\varepsilon_i$ and the optical thickness of the gold layer d(Au).

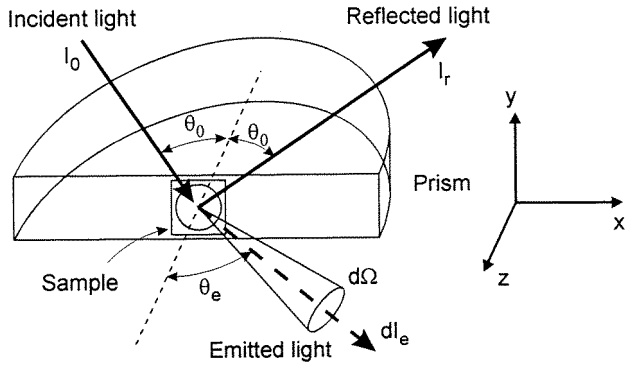

Figure 1. Optical scheme of ATR excitation of surface plasmon mediated rear-side light emission. θ_0—resonant angle of excitation, θ_e—angle of emission.

Surface plasmons of the gold/air interface emit light into the open rear hemisphere when scattered on the natural surface corrugations of the sample (figure 1). Maximum light intensity was given when the excitation was at θ_0. The intensity $\mathrm{d}I_e$, emitted into the solid angle dΩ (determined by the size of the Si detector), was measured in the plane of excitation (x–z) as a function of the angle of emission θ_e. This angle was measured from the surface normal of the metal film and was taken to be positive in the hemisphere containing the plasmon vector [2].

The emission efficiency $\eta_e = I_e/I_0$ was measured separately using a large area (10×20 mm^2) silicon PIN diode (Hamamatsu S2744-04) placed close to the gold film. (I_e—total emitted light into 2π solid angle, I_0—non-reflected part of the incident laser beam.) The estimated experimental error calculated from the angular dependence of the detector was less than 10%.

3. Results and discussion

3.1. ATR reflectivity measurements

Figure 2 shows the change of the ATR reflectivity at $\lambda = 632.8$ nm as a function of the LiF thickness. The minimum reflectance shifted to larger θ values and the angular width of the curves increased up to d(LiF) $\approx$ 400 nm, then both again approach the d(LiF) = 0 case. The sample with d(LiF) = 500 nm behaves like one with d(LiF) = 150 nm. A similar saturation phenomenon was reported in [3] for thick LiF layers determined by transmission electron micrography.

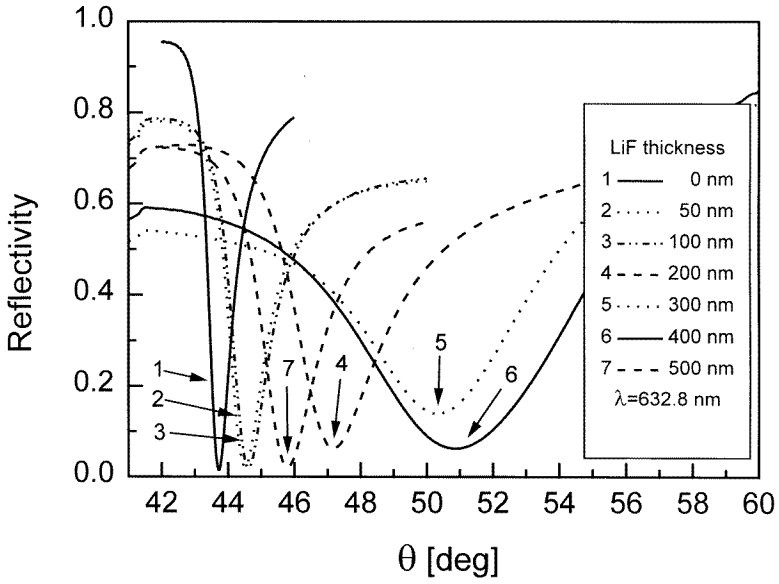

Figure 2. ATR reflectivity of samples with LiF sublayers of different thickness, covered with 50.4 nm gold, ($\lambda = 632.8$ nm).

The observed shifts in θ and the increase in the angular width of R–θ resonance dips indicate the scattering of surface plasmons. Their wave-vector $\tilde{k} = k_r + \mathrm{i}k_i$ was found to have changed drastically with increasing roughness amplitude; k_r was shifted to longer values (i.e. plasmons became 'slower'); k_i, which is proportional to the width of the resonance curve, also increased, indicating a decrease in plasmon lifetime.

$$k_r = nK \sin\theta_0 \tag{1}$$

$$k_i = \Delta k_{HWHH} \tag{2}$$

where n is the refractive index of the prism, $K = 2\pi/\lambda$ the wave-vector of the incident light with vacuum wavelength λ, and Δk_{HWHH} the half width of dips in figure 2 in k units. The momentum changes Δk_r and Δk_i, calculated from the parameters of reflectivity curves of $d(\mathrm{LiF}) = 0$ and $d(\mathrm{LiF}) > 0$, are plotted in figure 6(a).

Evaluation of the optical constants for Au was carried out from the reflectivity data using Fresnel's equations of a four-layer system, *viz.* glass–LiF–Au–air [4]. Refractive indices of LiF layers were assumed to be equal to the bulk values. Bulk indices were determined with total reflection measurements on an LiF single crystal and were found to be $n = 1.393$ and 1.385 at $\lambda = 632.8$ and 1064 nm, respectively. The fitting was excellent for the $d(\mathrm{LiF}) = 0$ sample and the gold thickness was determined as $d(\mathrm{Au}) = 50.4$ nm, which agrees within 1% error with the x-ray small angle scattering thickness value. Dielectric constants for the other samples were determined assuming this thickness value remained unchanged. Table 1 contains the complex ε values for two wavelengths. These values are, of course, unrealistic for the gold layer if $d(\mathrm{LiF}) > 0$ nm. They reflect, however, the change of surface plasmons as a consequence of the scattering on surface roughness produced in the gold by the micro-structure of LiF sublayers. Although it would be straightforward to determine the roughness spectrum directly from the ATR curves, up till

Table 1. Dielectric function values of 50.4 nm gold layer deposited on substrates previously coated with LiF layers of different thickness.

	λ = 632.8 nm		λ = 1064 nm	
d_{LiF} [nm]	ε_r	ε_i	ε_r	ε_i
0	−12.61	1.2	−51.02	2.2
50	−9.88	1.4	−39.85	1.4
100	−9.66	1.4	−39.87	1.6
200	−5.40	0.8	−27.31	0.9
300	−3.97	0.7	−20.82	0.7
400	−3.84	0.8	−20.01	0.8
500	−7.24	1.0	−31.73	1.0

now no theory exists which would include the scattering of surface plasmons in Fresnel's equations.

3.2. Light emission measurements

From ATR optical measurements the only possibility to obtain information for the roughness is to analyse the angular distribution of the rear-side light emission.

In the simple case, when the surface modulation of the sample consists of parallel, y-direction sinusoidal lines (i.e. gratings) with period a, surface plasmons which propagate along the x-direction in the x–y plane of the metal film will be scattered by this modulation and emit light. The wave-vector change is given as

$$\Delta k = K(n \sin\theta_0 - \sin\theta_e) = mG \tag{3}$$

where $G = 2\pi/a$ is the grating vector, and $m = 1, 2, 3, \ldots$ are integers.

In order to study this effect we measured the rear-side light emission from a 50 nm gold layer evaporated on a holographic grating substrate with period $a = 704$ nm and amplitude $h \approx 10$ nm. Figure 3 shows that emission angle θ_e is at 8.7° if $m = 1$ and the second order scattering ($m = 2$) appears at −49°. (This is equivalent with the first order scattering from an $a' = a/2$ grating, as the upper scale shows.) The angular width of the scattered lines is determined by the finite (3×3 mm^2) size of the Si detector. Their natural width is about 0.5°.

The gold samples evaporated on LiF sublayers show random, stochastic roughness distribution which, in the optimal case, is isotropic in the plane of the substrate. In this case the surface plasmon induced light emission does not obey discrete lines, but wide maxima (figure 4). In order to compare the scattering of plasmons on periodic and random corrugations, we constructed the scale of 'effective' (i.e. sinusoidal) periods from (3) using the experimental Δk values.

Applying first order perturbation treatment of the plasmon scattering on small amplitude ($\delta \leqslant 1$ nm) random roughness the emitted intensity is given by [5]

$$I_{rel} = \frac{\mathrm{d}I_e}{I_0\,\mathrm{d}\Omega} = 4\left(\frac{\pi}{\lambda}\right)^4 \frac{n}{\cos\theta_0} |t_p(\theta_0)|^2 |W(\theta)|^2 |S(\Delta k)|^2 \tag{4}$$

where $|t_p(\theta_0)|^2$ is Fresnel's transmission coefficient of the four-layer system, $|W(\theta)|^2$ the dipole radiation function of the surface and $|S(\Delta k)|^2$ the spectral density function of the roughness. From the viewpoint of evaluating the roughness spectrum, this latter function

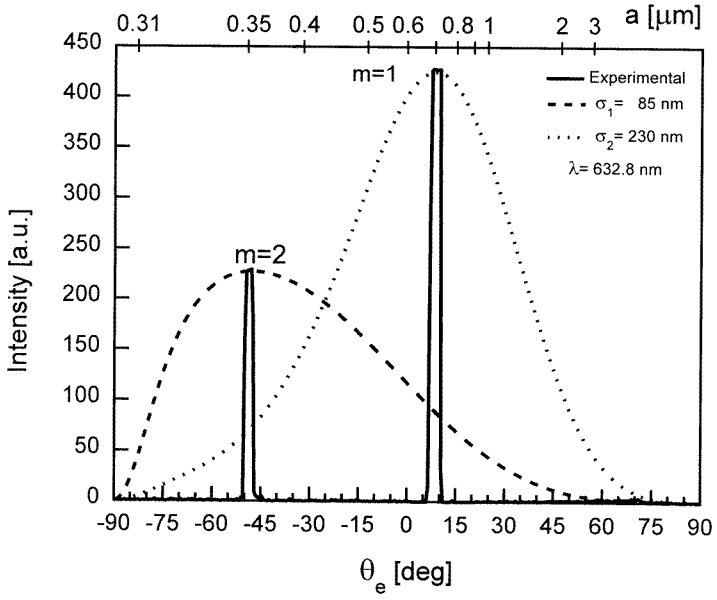

Figure 3. Rear-side light emission from a 50 nm gold layer deposited on holographic grating with $a = 704$ nm period. Continuous line: surface plasmon diffraction in first and second order. The peak width reflects detector size. Dotted line: theoretical calculation using (4).

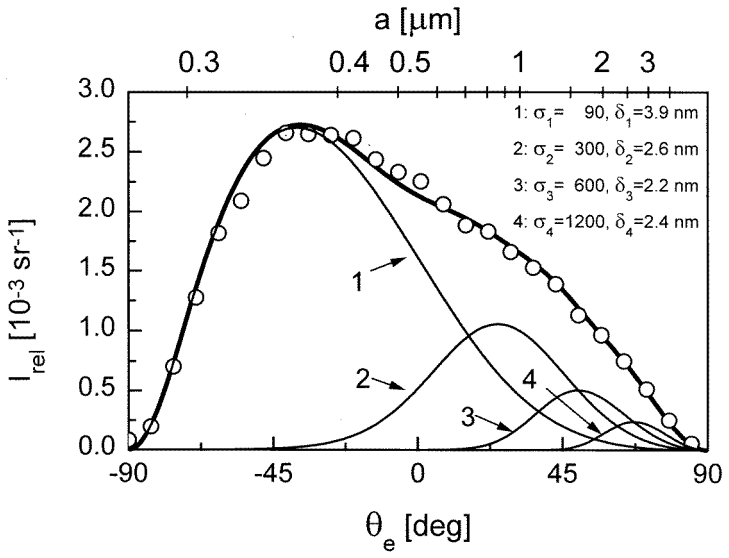

Figure 4. Angular distribution of rear-side light emission of sample with 300 nm LiF sublayer covered with 50 nm gold at $\lambda = 632.8$ nm. The scale of 'effective' periodicity of roughness a was determined from momentum change Δk using (3). The roughness parameters (σ, δ) were calculated by (4), based on perturbation theory [5]. Continuous line: calculated curves; circles: experimental points.

is the most important for us. If the rough profile of the surface is given by function $z = S(x, y)$ and the zero level is given by the condition $\int S(x, y)\,\mathrm{d}x\,\mathrm{d}y = 0$, the definition

of the autocorrelation function of the surface is [5]:

$$G(x, y) = \frac{1}{F}\int_F S(x', y')S(x' - x, y' - y)\,\mathrm{d}x'\,\mathrm{d}y' \tag{5}$$

where F is the surface of the sample. With Gaussian approximation

$$G(x, y) = \delta^2 \exp\left(-\frac{x^2 + y^2}{\sigma^2}\right) \tag{6}$$

where σ is the correlation length and δ the rms amplitude of the roughness. These are the parameters we need to determine from the light emission of the rear-side.

Because the intensity measurements were made only along the x direction (figure 1), we should restrict our calculations to one dimension. In this case (6) gives $\delta^2 = G(x = 0) = G_0$ and $\sigma = x$ at that value where $G(x) = G_0/\mathrm{e}$. The Fourier transformation of (6) gives

$$|S(\Delta k)|^2 = \frac{1}{4\pi}\sigma^2\delta^2 \exp\left(-\frac{\sigma^2(\Delta k)^2}{4}\right) \tag{7}$$

which is the most important equation for practical use.

Generally, the roughness of a sample cannot be given by a single (σ, δ) parameter pair. If corrugation components are independent [6]:

$$|S(\Delta k)|^2 = \sum_i |s_i(\Delta k)|^2 \tag{8}$$

where usually $i = 1$–8, and every component has different (σ, δ) parameters which are valid only within a certain Δk region.

In practice we used the linearized form of (7) and (8) to evaluate the roughness parameters:

$$\ln|s_i(\Delta k)|^2 = \ln\left(\frac{\delta_i^2\sigma_i^2}{4\pi}\right) - \frac{\sigma_i^2(\Delta k)^2}{4}. \tag{9}$$

The experimental $|S(\Delta k)|^2$ function was determined from (4) using the experimental I_{rel} emission intensity, the calculated Fresnel coefficient and the dipole radiation function [5]. The function values were plotted against $(\Delta k)^2$, which was calculated from (3) (figure 5). The large Δk part of the curve was fitted with a straight line. Parameters (σ_1, δ_1) were obtained from the slope (M) of this line and from its extrapolated value to $(\Delta k)^2 = 0$:

$$\sigma = 2\sqrt{M} \qquad \text{and} \qquad \delta = \sqrt{\frac{\pi}{M}|s(\Delta k)^2|}\bigg|_{\Delta k=0}. \tag{10}$$

This straight line (1) was subsequently subtracted from the experimental curve and the remaining part was approximated by line (2). This gave parameters (σ_2, δ_2). The method can be continued until the experimental error near to $\Delta k = 0$ gives too large uncertainties.

The parameters determined by this graphical method were slightly corrected in order to obtain the best fit of the experimental points in figure 4 using (4). Our view is that with this method at least the most important first two to three components were exactly determined. The less dominant others (where $\sigma > 500$ nm) are somewhat arbitrary in σ.

Similar σ parameters were found with an analogous experimental technique for silver covered LiF samples of $d(\mathrm{LiF}) \leqslant 200$ nm thickness [7].

The results for height (δ) from surface roughness analysis up to the fourth component together with surface plasmon wave-vectors, calculated from (1) and (2) and the overall brightness of the emission η_e are plotted in figure 6(a). Experimental values were, for the sake of clarity, spline fitted, which slightly rounded off the abrupt change of parameters

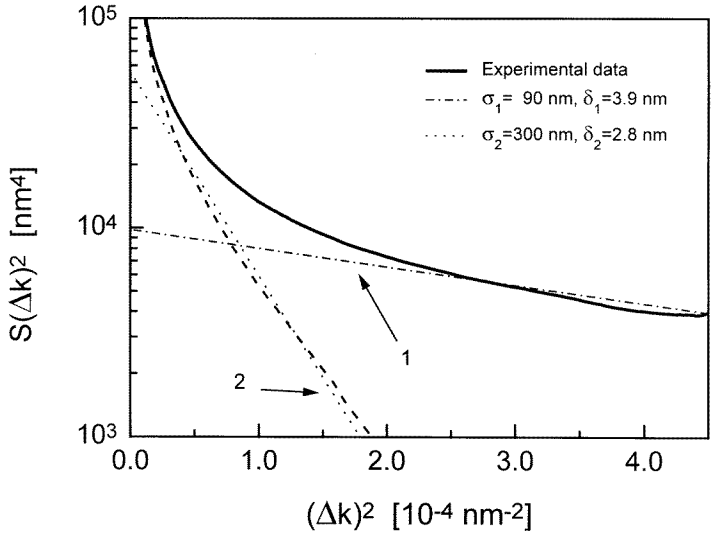

Figure 5. Graphical method of calculation of roughness parameters from experimental data for a 50 nm Au film on 200 nm LiF sublayer. $\lambda = 632.8$ nm. Lines 1 and 2 give parameters (σ_1, δ_1) and (σ_2, δ_2), respectively. Dashed line represents experimental data with (σ_1, δ_1) contribution removed.

between 350 and 400 nm. These data, together with the change of dielectric functions (table 1) indicate a saturation of roughness amplitudes at 350 nm and, further, for greater LiF thickness, a flattening out of the corrugations of the film.

The physical meaning of the roughness amplitude (δ) is clear. However, the correlation length (σ), as defined by (6), is definitely not equal to the average distance between corrugations (grains, hillocks, crystallites etc), which can easily be determined from AFM/STM pictures or from electronmicrographs.

In order to check the validity of roughness calculations based on (4)–(10) for regularly corrugated systems, we examined two cases. First, for a linear holographic grating we tried to analyse the rear-side emission within this model. Our calculations resulted in very wide maxima with $\sigma_1 = 85$ nm and $\sigma_2 = 230$ nm (instead of 352 nm and 704 nm, respectively). These correlation lengths are three to four times smaller than the actual grating periods (figure 3).

In the second case we used (5) and (6) to analyse a close packed planar array of uniform spheres, e.g. latex balls (figure 7(a)). The autocorrelation function is demonstrated as a contour map in figure 7(b). At the origin (centre of the figure) the $G(x, y)$ function was normalized to be unity, and the σ values can be found along the $G \approx 0.37$ line. The correlation lengths are almost symmetrically $\sigma \approx a/5$ in every direction while in the figure $a = 50$, the diameter of a sphere.

Both cases demonstrated that the model utilized for periodic systems resulted in correlation lengths $\sigma < a/3$, which are very different from the size of the corrugations a.

The AFM analysis of LiF samples gave $\sigma \geqslant d/2$, i.e. the correlation length and the average grain size (d) were similar (figure 6(b)). Consequently, in perfect, randomly corrugated systems $\sigma \sim d$ could be expected. We would mention that even in this case the Δk momentum transfer, responsible for the largest emission peak (σ_1) in figure 4, corresponds to a much larger 'effective' scattering period ($a \sim 360$ nm) than the grain size

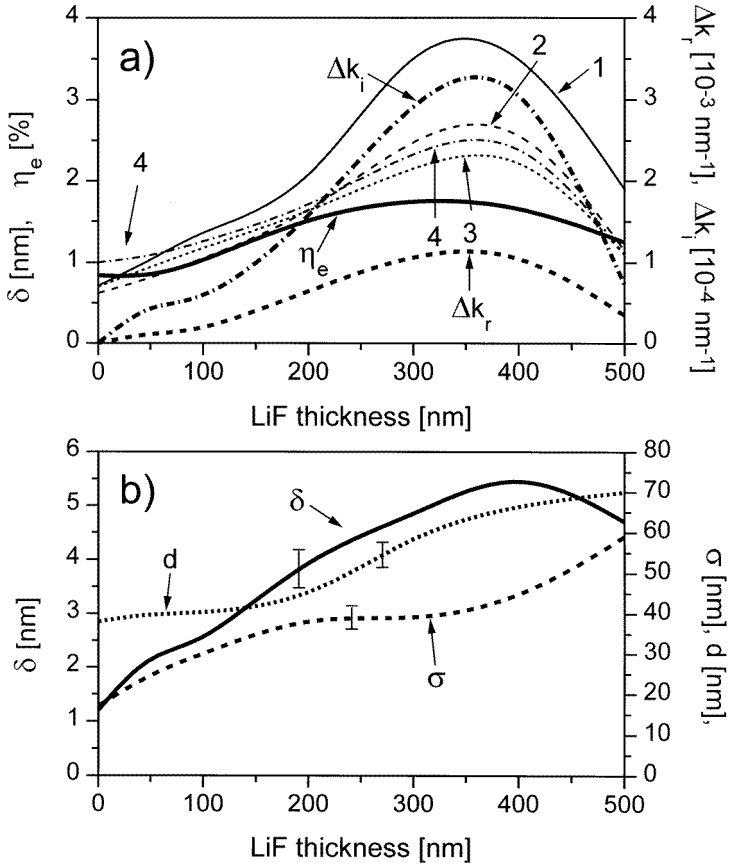

Figure 6. Results for Δk_r, Δk_i, δ_1, δ_2, δ_3, δ_4 and η_e for samples with LiF of different thickness. Experimental points are spline fitted for the sake of clarity. Deviation of measured points from the fit is less than $\pm 5\%$. (a) Optically determined parameters at $\lambda = 632.8$ nm. (b) σ, δ and average grain diameter d determined by AFM.

or σ. We consider this to be a consequence of interference effects between surface plasmon waves scattered by corrugations of very wide distribution.

3.3. AFM measurements

All samples were checked by an AFM of Nanoscope III type. LiF samples showed well defined, random hillocks of different height (figure 8). The average crystallite size (d) was determined from two-dimensional pictures. The (σ, δ) pairs of the roughness were calculated using several x and y cuts of three-dimensional pictures and analysed using (5) and (6).

The d, σ and δ parameters were determined as an average of several (sometimes up to 30) different pictures because the picture size was only 1×1 μm^2, while for optical measurements we used a 1 mm diameter laser beam, i.e. averaging was done over a 10^6 times larger area.

AFM parameters are plotted in figure 6(b). The average grain size (d) and σ increase monotonically with the thickness of LiF whereas the roughness amplitude (δ) begins

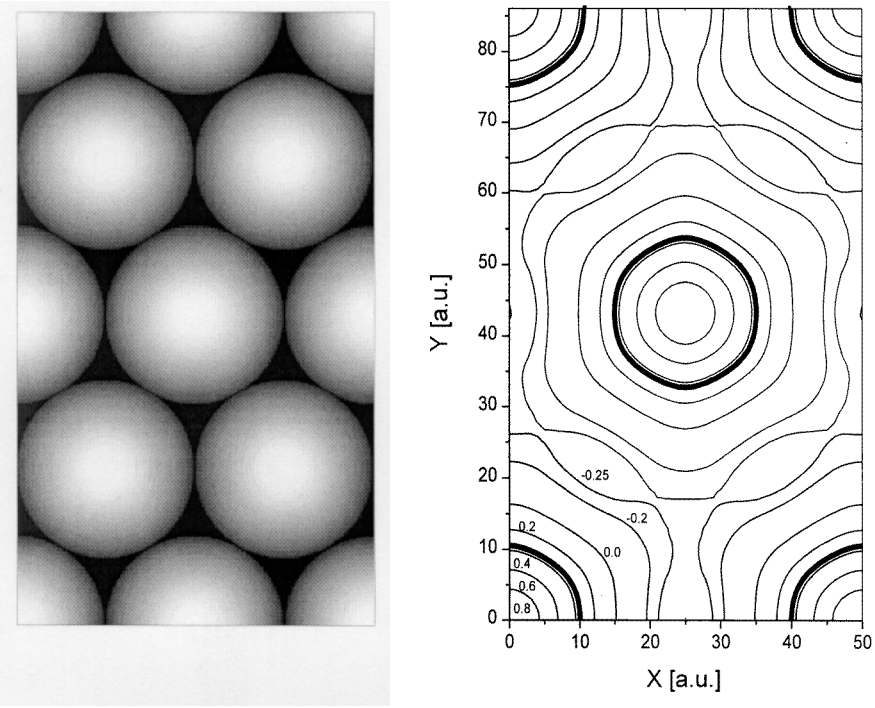

(a) (b)

Figure 7. Close-packed planar array of uniform spheres with diameter $a = 50$ units (a) and autocorrelation function of this grating (b). σ is almost circular with a value $\sigma \approx a/5$ (thick line).

to decrease between 350 and 400 nm, in accordance with the optical measurements (figure 6(a)). The AFM correlation length was $\sigma = 40 \pm 20$ nm in the whole region, which is—in the sense of the above described calculations—near to the optically determined shortest component $\sigma_1 \approx 90$ nm and very close to the average grain size $d = 60 \pm 10$ nm. It means that optical and AFM measurements give similar results, and that the LiF system shows *random* roughness distribution.

Grain size and corrugation parameters were found to depend strongly on the rates of condensation for both LiF and Au, in accordance with [8].

4. Conclusions

Comparison of ATR based optical and AFM measurements of artificially (with LiF sublayers) roughened gold samples shows satisfactory agreement between roughness parameters σ and δ despite the fact that the first order perturbation model is valid only for very small corrugation amplitudes.

We have introduced a new, graphical method to evaluate the σ parameters, and find that it gives less arbitrary values than the simple decomposition technique.

It was demonstrated by calculations that for one- and two-dimensional *periodic* systems the random distribution dipole radiation model gives, at least for the correlation length, wrong results.

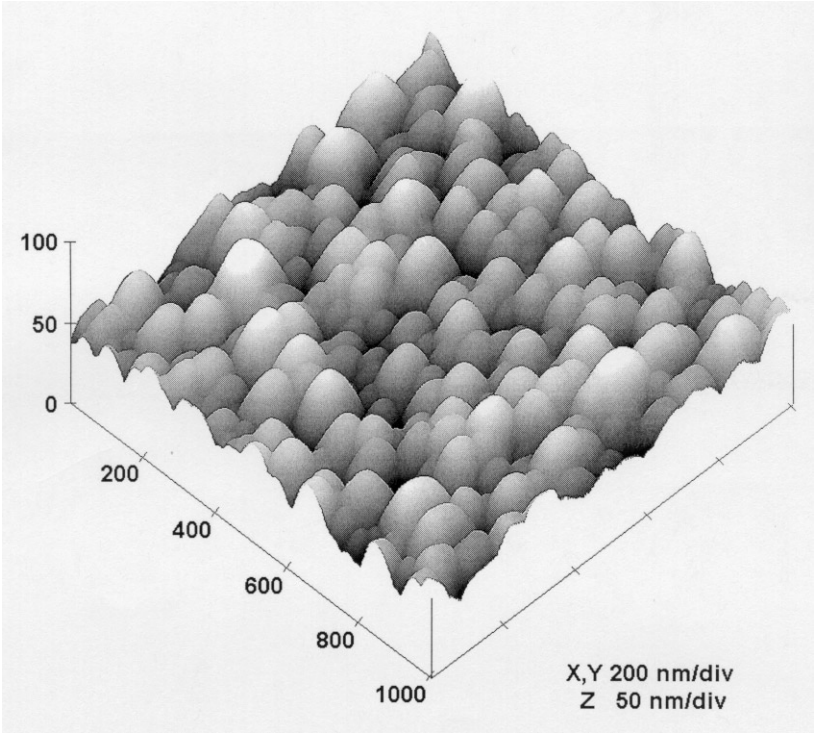

Figure 8. Three-dimensional AFM micrograph of 500 nm LiF film evaporated on glass substrate.

Using two independent experimental methods we confirm that LiF layers flatten out above a thickness of 350 nm. This saturation value should be a function of evaporation parameters [3]. We found correlation between LiF grain size, AFM correlation length and the shortest optically determined correlation length component σ_1. The change of roughness parameters as a function of thickness showed a similar tendency as reported in the literature [3]: continuous increase in σ and a saturation followed by a decrease in δ above some thickness value. Up till now, change of grain size has not been dealt with in the literature. Analysis of the published electronmicrographs resulted in LiF grain size between 40 and 60 nm for layers of 200–500 nm thickness [3, 9], in good agreement with our results.

The complex dielectric function of a gold layer shows drastic variations as a function of the roughness amplitude. This was checked at two wavelengths. Surface plasmons at the gold/air interface shift to larger values both in k_r and k_i. These phenomena cannot be described by the recent state theories available in the literature (e.g. [10]), although efforts were made to explain the changes in surface plasmon assisted light emission spectra with variations in k_i, induced by the morphology of the top gold electrode of Al–I–Au tunnel structures [8].

Acknowledgments

This work was supported by the Hungarian National Scientific Foundation (OTKA) under contract Nos T-16075, T-20089 and T-220074.

References

[1] Kretschmann E 1971 *Z. Phys.* **241** 313
[2] Hoffmann A, Kroó N, Lenkefi Z and Szentirmay Z 1996 *Surf. Sci.* **352–4** 1043
[3] Varnier F, Nayani N and Rasigni G 1989 *J. Vac.Sci. Technol.* A **7** 1289
Mayani N, Varnier F and Rasigni G 1990 *J. Opt. Soc. Am.* A **7** 191
[4] Boardman A D 1982 *Electromagnetic Surface Modes* (New York: Wiley) p 32
[5] Kröger E and Kretschmann E 1970 *Z. Phys.* **237** 1
[6] Naoi Y and Fukui M 1989 *J. Phys. Soc. Japan* **58** 4511
[7] Tajima H, Haraguchi M and Fukui M 1995 *Surf. Sci.* **323** 282
[8] Ferguson A J L, Walmsley D G, Hagan H P, Turner R J and Dawson P 1989 *J. Phys.: Condens. Matter* **1** 7931
[9] Cosset F, Celerier A, Bareland B and Vareille J-C 1997 *Thin Solid Films* **303** 191
[10] Brown G, Celli V, Haller M, Maradudin A A and Marvin A 1985 *Phys. Rev.* B **31** 4993